Optical Fiber Sensors for Spacecraft: Applications and Challenges

E. Joseph Friebele*[a], Charles G. Askins[a], Gary A. Miller[b], John R. Peele[a] and
Lucienne R. Wasserman[b]
[a]Naval Research Laboratory, 4555 Overlook Ave. SW, Washington, DC, USA 20375
[b]SFA, Inc., 9315 Largo Drive West, Suite 200, Largo, MD 20774 USA

ABSTRACT

Optical fiber sensors offer a number of advantages for spacecraft applications, including freedom from electromagnetic interference, light weight, and low power consumption. One application is strain sensing, where high sensitivity and bandwidth and the ability to individually interrogate tens of multiplexed sensors via a single fiber lead has been demonstrated. This paper will describe 2 recent NRL uses of distributed strain sensing using arrays of fiber Bragg gratings (FBGs) on spacecraft parts, structures, and ground test hardware: distributed dynamic strain monitoring of a lightweight reflector during acoustic qualification tests and high-frequency, high-sensitivity strain measurements of a latch fixture. A second fiber sensor being seriously considered for spacecraft is the interferometric fiber optic gyroscope (IFOG). Although its performance in a benign environment is quite attractive, deployment of this and other optical fiber sensors requires addressing issues such as the deleterious effects of the space radiation environment. These challenges, unique to this application, will be discussed.

Keywords: Fiber optic sensors, interferometric fiber optic gyroscope, space radiation, fiber Bragg gratings, strain sensing

1. INTRODUCTION

The viability of optical fibers in space has been proven in experiments dating back to the 1980's when a fiber optic systems experiment comprising 4 active data links was flown by Taylor of the former Air Force Weapons Laboratory (now known as the Air Force Research Laboratory) at Kirtland AFB, NM[1] for 69 months onboard the Long Duration Exposure Facility (LDEF). This experiment was the first known long-term deployment of operational optical fiber data links in space and demonstrated that the fibers could survive the space environment and radiation doses of up to 25 krad.

In the same time period as the recovery and analysis of the AFWL LDEF experiment, K. LaBel and coworkers at NASA-Goddard Space Flight Center developed a first-generation spacecraft fiber optic data bus based on MIL-STD-1773[2]. This system, which operated at 1 Mbs using multimode fiber at 850 nm, was first flown on the Solar Autonomous Magnetospheric Particle Explorer (SAMPEX) and successfully operated on several other spacecraft, including the X-ray Timing Experiment (XTE), Tropical Rainfall Measuring Mission (TRMM), and the Hubble Space Telescope (HST). A second-generation, dual data rate (1 and 20 Mbs) data bus, based on MIL-STD-1773A using single mode fiber operating at 1300 nm was subsequently developed by NASA-GSFC and flown on the Microelectronics and Photonics Test Bed. Bit error rate data were acquired from this experiment for ~4 years, between 1997-2003. Other spacecraft optical fiber systems include encoder, point-to-point systems, and a 100 Mbs FDDI system onboard the International Space Station. These and other successful applications have firmly established the viability of optical fibers for spacecraft data transmission.

In addition to the data transmission systems described above, there are other potential applications of optical fibers as sensors onboard spacecraft or spacecraft structures. Optical fiber strain sensing is a well-known technology, where fibers can be used for strain measurements *both* during testing and space qualification and while in service. Demonstrated examples include strain mapping, determination of deflection, deformation and shape, vibration detection and suppression, micrometeorite detection and classification, and distributed temperature measurement. A second promising application of optical fiber sensing in space is the interferometric fiber optic gyroscope (IFOG). Here, a long

Photonics for Space Environments IX, edited by Edward W. Taylor,
Proceedings of SPIE Vol. 5554 (SPIE, Bellingham, WA, 2004)
0277-786X/04/$15 · doi: 10.1117/12.562393

length coil of polarization-maintaining single mode fiber in a Sagnac interferometer is used as a rotation sensor, and Er-doped fiber is used in the broadband fiber light source. Although there has been a significant amount of work in fiber sensors for spacecraft, this paper is not intended as a review, but rather to highlight recent NRL demonstrations in distributed strain sensing on spacecraft parts and to discuss potential issues regarding the deployment of IFOGs in the space radiation environment.

2. FIBER BRAGG GRATING ARRAYS FOR SPACECRAFT STRAIN SENSING

The technology of strain sensing using fiber Bragg gratings (FBGs) has been thoroughly discussed by Kersey et al.[3], and the preliminary application of this technology to spacecraft structures is described in a previous article by Friebele et al.[4] FBGs have been selected for sensing static or dynamic strain on spacecraft structures because of the unique advantages they offer, including (and in approximate order of priority): 1) The fact that FBGs can be multiplexed into multi-element arrays for distributed sensing where >100 sensors can be simultaneously interrogated by one instrumentation package at high speed with no time skew between individual sensor measurements; 2) The FBGs are small, light weight and can be mounted in spaces with tight clearances; 3) Absolute strain measurements can be made using FBGs without constant monitoring since strain is encoded as wavelength shift; 4) Glass optical fibers with polymer coatings (both dielectric materials) are immune to electromagnetic interference and crosstalk; 5) Fibers are compatible with a wide range of structural materials (fiber reinforced polymer composites, metals, etc.); and 6) Fiber arrays can be surface mounted with spacecraft-qualified adhesives or embedded in the structure itself.

2.1. FBG instrumentation of a lightweight antenna reflector

The preliminary application of FBGs to monitor a lightweight antenna reflector during acoustic qualification testing for flight has been described in reference 4. This initial demonstration on the prototype reflector showed that FBG sensors offered a number of advantages, including ease of application, small size, inconsequential mass-loading, minimal leads, and immunity to electrical noise, while providing strain information in many ways superior to that reported by conventional resistance strain gages (RSGs). As a result of that experiment, NRL was tasked to perform more extensive instrumentation of a flight article reflector to assist in structural design verification. The sensor configuration included 40 FBGs located at high-strain locations. Figure 1 shows the reflector with five circled sensor placement areas and insets detailing the attachment points. Figure 1(b) is a close-up of one of the circled regions on the full-scale diagram. A metal junction mates two small graphite struts to the support ring tube. The five metal junctions chosen for instrumentation are closest to three underlying fixtures that mount the entire reflector to the test fixture and are therefore expected to experience the highest strains. Figures 1(a) and 2 show a cross section of one of the two struts of inset Fig. 1(b) with properly scaled FBG sensors surface-mounted at each of the four edges (only the grating regions, not the intervening leads are indicated). It was desired to place strain sensors along the vertices of the struts, very close to the metal junction, to closely resolve maximum bending moments as well as axial strain components. Because of the struts' small cross section (approximately 5 x 3 mm), as shown in Figure 2, the geometry of an optical fiber was much better suited for attachment near the edges than a conventional RSG.

Because of the large number (40) of sensors, custom FBG arrays were produced on-line during the fiber draw process[5]. The bandwidth of the light source and the anticipated strain range of +2500 $\mu\varepsilon$ meant that only eight WDM channels could be illuminated. Thus, five separate fibers were required to instrument all 40 locations. A single fiber was configured to place one FBG at each of the eight locations shown in Figure 1(b), four on each of two struts. Because the reflector was a flight structure, the sensors were attached with a flight-qualified epoxy (Dexter Hysol EA 9394). A specialized clamp held four FBGs under slight tension along each strut at the intended sensor locations until the epoxy could be applied and set.

In contrast with the "proof-of-concept" demonstration completed on the prototype article in 1996 and described in reference 4, the sensors on the flight article were interrogated with a different instrument capable of more channels and absolute (dc) strain measurements. The earlier method employed a wavelength-multiplexed interferometric approach with a modulated carrier, while an imaging CCD spectrometer instrument[6] was used to interrogate the flight article sensors. To accommodate the requirements of the latter test, the central imaging element was increased from 256 to 512 pixels, and the clock rate increased by 25%. This enabled a broader spectrum to be monitored. Calculations indicated that structural deflections during acoustic qualification testing could result in strains of ± 2500 με, which limited the number sensors per array to 8 to avoid coincidence or crossing of the FBG peaks. To achieve the broad input spectrum required for monitoring 8 sensors each with a ± 2500 με range, the outputs of a pair of diode light sources with relatively narrow spectral widths were combined through a fiber coupler. A fiber optic switch, which was used to select the 8-element array for interrogation, was required to acquire data from all 40 sensors. The system, shown schematically in Figure 3, allowed simultaneous interrogation of all 8 FBGs in one of the 5 sub-arrays at a data rate of 285 Hz. (C++ code was written to acquire the data at 2 kHz, but a hard disk failure required the use of a much slower acquisition program written in QuickBasic.) Sub-ppm (με) sensitivity was obtained using an NRL-patented algorithm[7] that achieved sub-pixel resolution of the peaks of the FBGs.

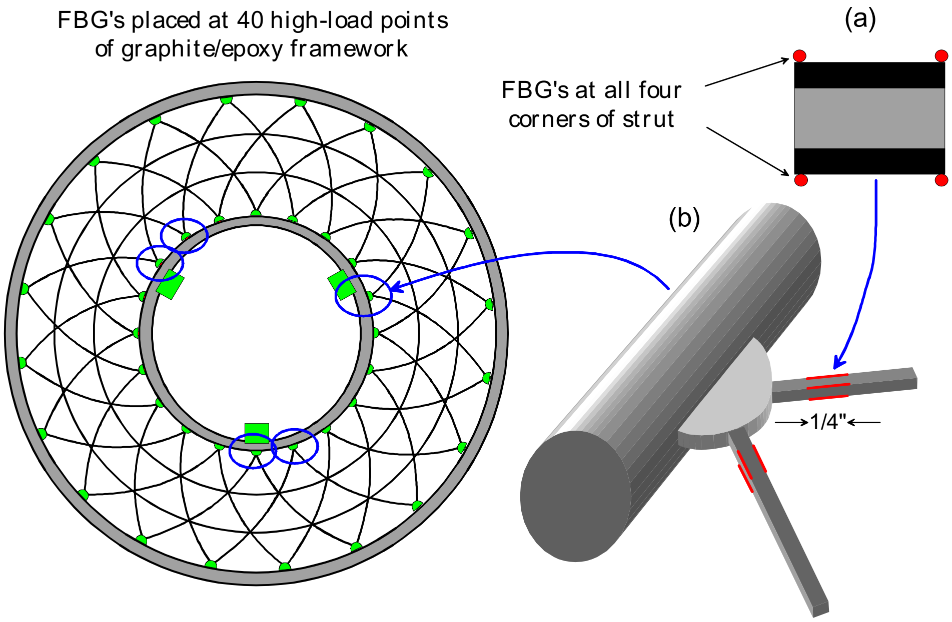

Figure 1. Schematic of the flight reflector structure showing the 5 locations where 8 FBG strain sensors were attached (ovals). The insets show the details of the attachment (a) in cross section and (b) from perspective.

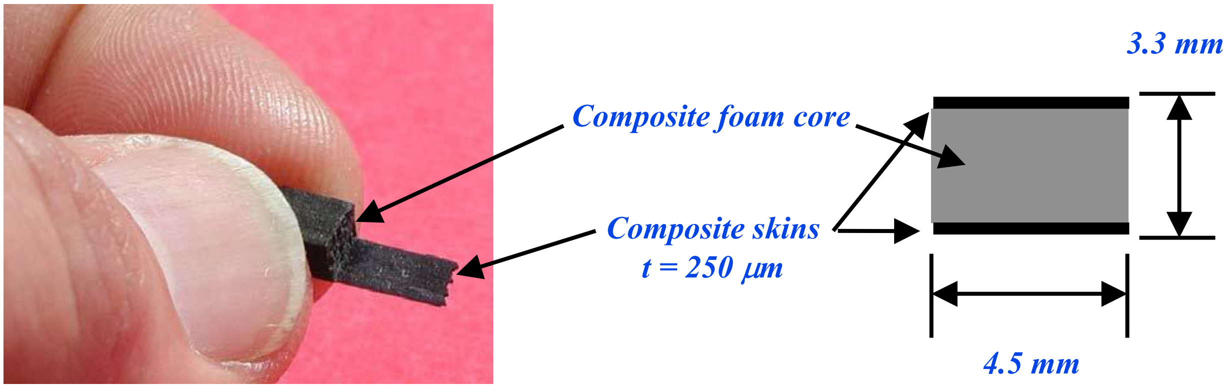

Figure 2. Picture showing the size of the composite strut and cross section showing dimensions.

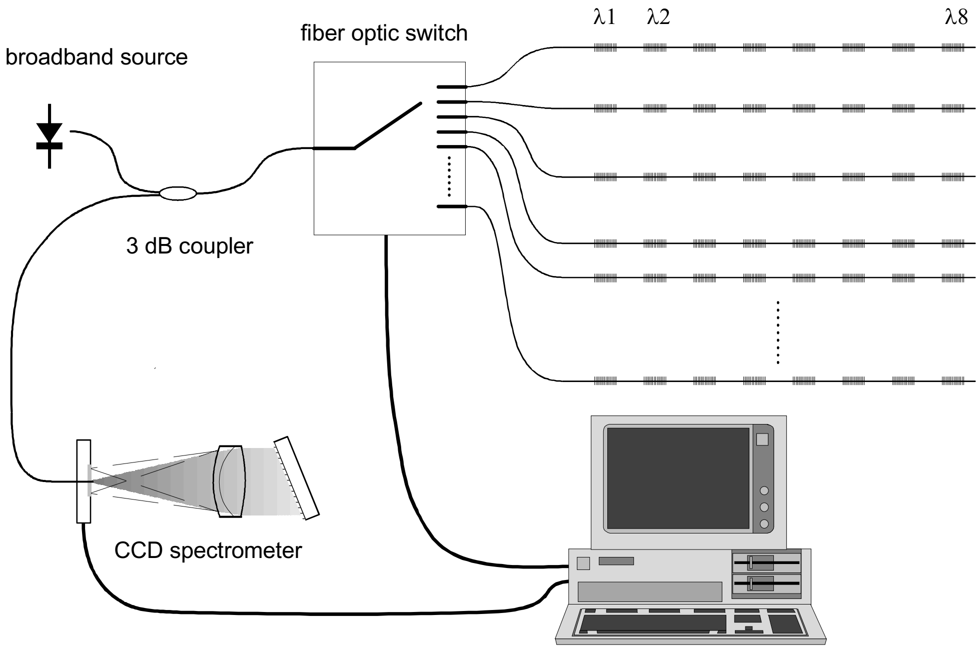

Figure 3. Schematic of the CCD spectrometer system for interrogating the 8-element FBG arrays attached to the antenna reflector flight article. The switching time of the fiber optic switch was ~0.1 s.

The positions of the sensors on the flight article are shown in Figure 4, and data collected from one 8-element FBG sensor array during the 146 dB acoustic loading test are shown in Figure 5. The signals provide high fidelity strain records for all eight sensors. The data from sensor groups (5-8), (3-4), and (1-2) are well correlated. To examine the data in detail, the right-most 50 milliseconds of data have been expanded. It is apparent that FBGs (5-6) are anti-correlated with (3-4). This can be interpreted as a bending of strut H perpendicular to the membrane (see Figure 5). The different behaviors of FBGs (1-2) and (3-4) indicate a more complex bending, perhaps due to the greater distance of strut I from the support ring clip or perhaps delamination between the core and the top composite skin, on which sensors (1-2) are mounted. Additional structural analysis is necessary to fully interpret these data.

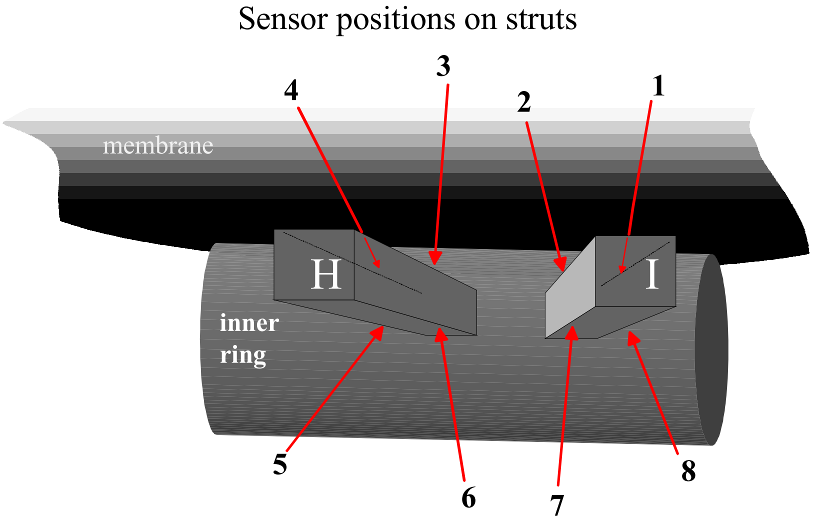

Figure 4. Schematic diagram of sensor positions on struts.

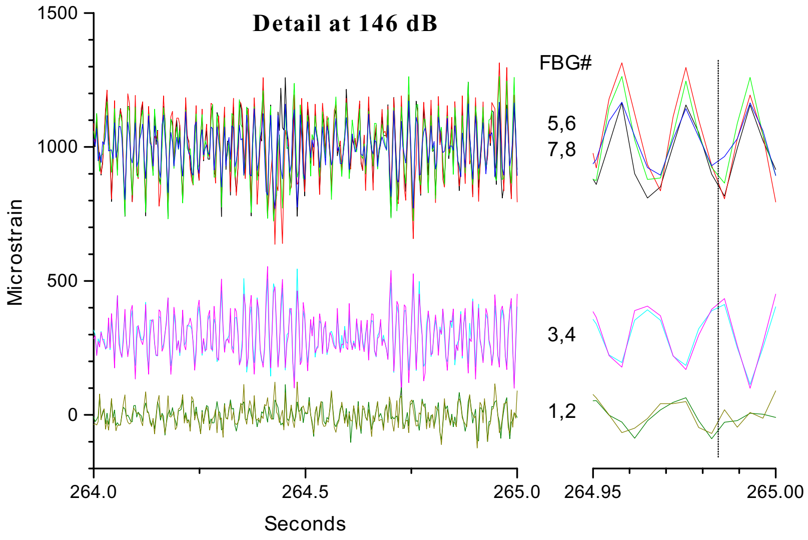

Figure 5. Detail of temporal strain data acquired during the acoustic test at 146 dB showing the good correlation between sensor sets 5-8 and 3-4. Possible reasons for the lack of correlation with sensors 1-2 are discussed in the text. Offsets have been added for clarity.

In addition to high fidelity dynamic strain information, the nature of the FBG sensor system employed for this test enables the comparison of absolute strain before and after the test and over the life of the structure. The initial spectra of the FBGs may be recorded along with a reference argon gas discharge spectrum (obtained from a penlight-sized source). The argon spectrum is constant over time and permits absolute calibration of the sensor signals. In this way, the strain state of the flight article can be tracked through subsequent assembly and testing stages, accompanied by a detailed map of structural changes on the ppm level. This is in sharp contrast to electronic strain sensors, which have significant drift over minutes or hours. Alignment tests that are performed after acoustic loading to evaluate deformation could easily be augmented by detailed strain mapping to identify and localize points of structural relaxation or damage.

In summary, we obtained high quality strain data during the acoustic test of the flight article. These data included measurements of the noise floor of the sensors, which was < 1με, measurements during the acoustic tests at 146 dB, and measurements of the pre- and post-test strain state (data not shown), which indicated damage to the strut.

2.2. Dynamic strain measurements of a spacecraft latch test fixture

A subsequent test supported the study of a spacecraft latch to establish its stiffness characteristics at low amplitude dynamic loads using the fixture shown in Figure 6(a). The vertical post was actuated by a shaker with various test loads, including random, burst random, sine decay, and low-level dither. The latch was mounted between the adapter bracket and the large bracket to the right of the drawing, which served as mechanical ground. Calculations indicated typical peak loads of ~0.5 - 2.5 kg at the latch. This load would induce strains of ~0.01 – 2.2 με in the adapter bracket where the FBG strain sensors were to be mounted. As shown in Figure 6(b), the adapter bracket had 4 legs between the vertical member and the latch mounting plate. Both bending (in two dimensions) and torsion had to be measured on each of the 4 legs. Two FBG strain rosettes were attached to the vertical post, and 2 additional FBGs were packaged as temperature sensors and attached to legs of the adapter plate. Figure 6(b) shows the position and orientation of the FBG sensors. The strain sensitivity required for the test was <1 με with simultaneous measurement (e.g. no time skew) of strain and temperature from all 24 FBGs at a 2 kHz sample rate. Additionally, because the test spanned several months, the interrogation system was left on-site and operated by personnel who were not experts in FBG strain sensing or the CCD spectrometer measurement system. Thus, it was necessary to develop a GUI interface for data acquisition based in LabView. However, to achieve the required 2 kHz data rate, the data processing to extract strain from the FBG spectra was accomplished with a C++ DLL in the LabView VI. This system, which provided real-time display of the grating array spectra or strain and the option to store both spectra and strain, was successfully operated by the test engineers for 5 months. Figure 7 shows the front panel of the post-processing VI, which is similar to that of the data acquisition VI.

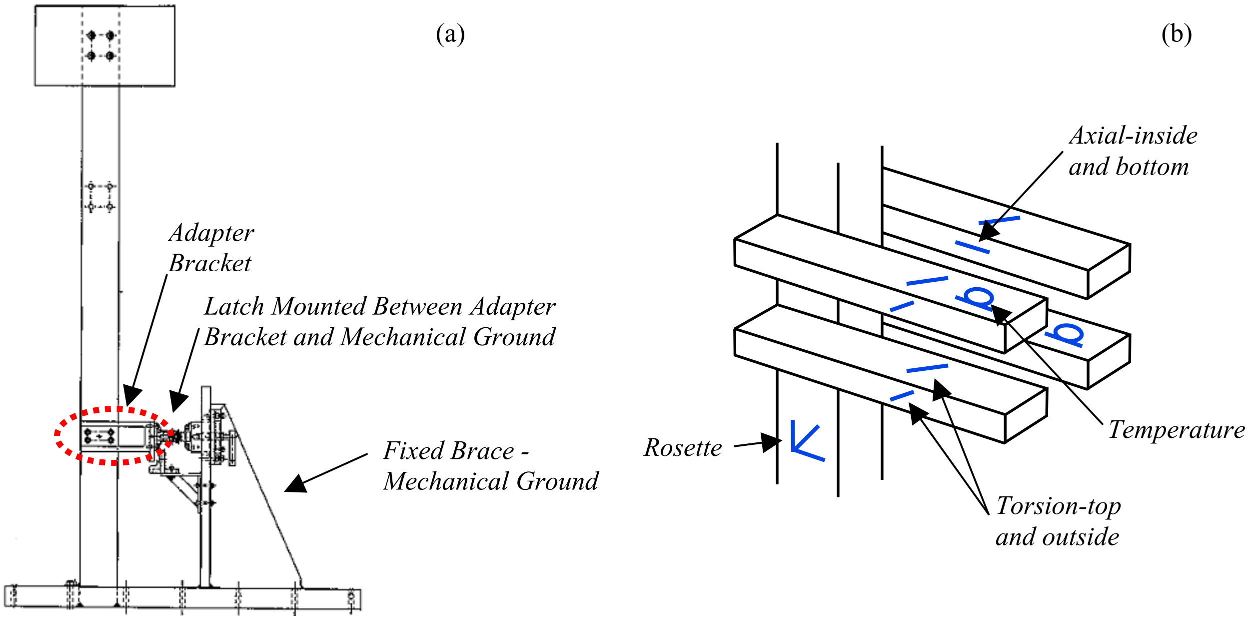

Figure 6. (a) Drawing of the spacecraft latch test fixture showing the adapter bracket where the FBG strain sensor array was mounted and (b) drawing of the adapter bracket with the latch mounting plate removed for clarity, showing the positions of the FBG strain and temperature sensors.

The FBGs used for this test were also made by exposing the fiber to a single pulse exposure of a UV excimer laser during fiber drawing.[5] A number of arrays consisting of 25-30 FBGs with different Bragg wavelengths were written during a single draw; the array chosen for this test consisted of 28 gratings spaced by 40 cm. Note that the Bragg wavelength of a grating is determined by the angle of the intersecting UV beams that write the grating and is set by computer-controlled turning mirrors in the writing interferometer. The lineal grating spacing is arbitrary, and the KrF UV writing laser is triggered by computer. Prior to installation, the strain and temperature responses of the grating sensors were measured using a cantilevered beam. The FBGs were attached to the adapter bracket with cyanoacrylic glue, which cured in a few seconds so that fixturing to hold the FBGs was not required. Unfortunately, there were several fiber breaks during installation; however, 21 FBG strain sensors and 2 packaged temperature sensors were successfully installed.

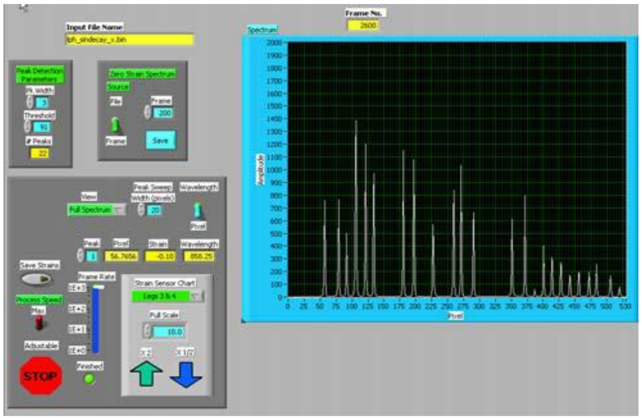

Figure 7. Front panel screen of the LabView post processing VI used for analysis of stored spectral data. The screen shows the spectrum of the installed FBG array. Both the data acquisition and post processing VIs can display either the array spectrum plotted vs. pixel number or wavelength, or strain as a function of time.

A massive amount of data was acquired over the 5 months of the test; two examples of sine decay are shown in Figure 8. Note the low system noise ±0.5 με evident in the traces prior to ~30 s of excitation. The ~125 s of strain data shown here were derived from 250,000 spectra of the FBG array; strain (or temperature) data were obtained for all 23 gratings of the array by real-time analysis of the spectra. Figure 8(a) shows decay after excitation of the vertical member in the x direction, i.e., along the horizontal axis of the adapter bracket, and the slow time constant indicates satisfactory stiffness in the latch. Figure 8(b) shows decay following torsional excitation, and the more rapid decay is indicative of less stiffness in torsion. Note from Figure 8(c) the slight temperature rise during excitation which is reported by the FBG temperature sensor packages.

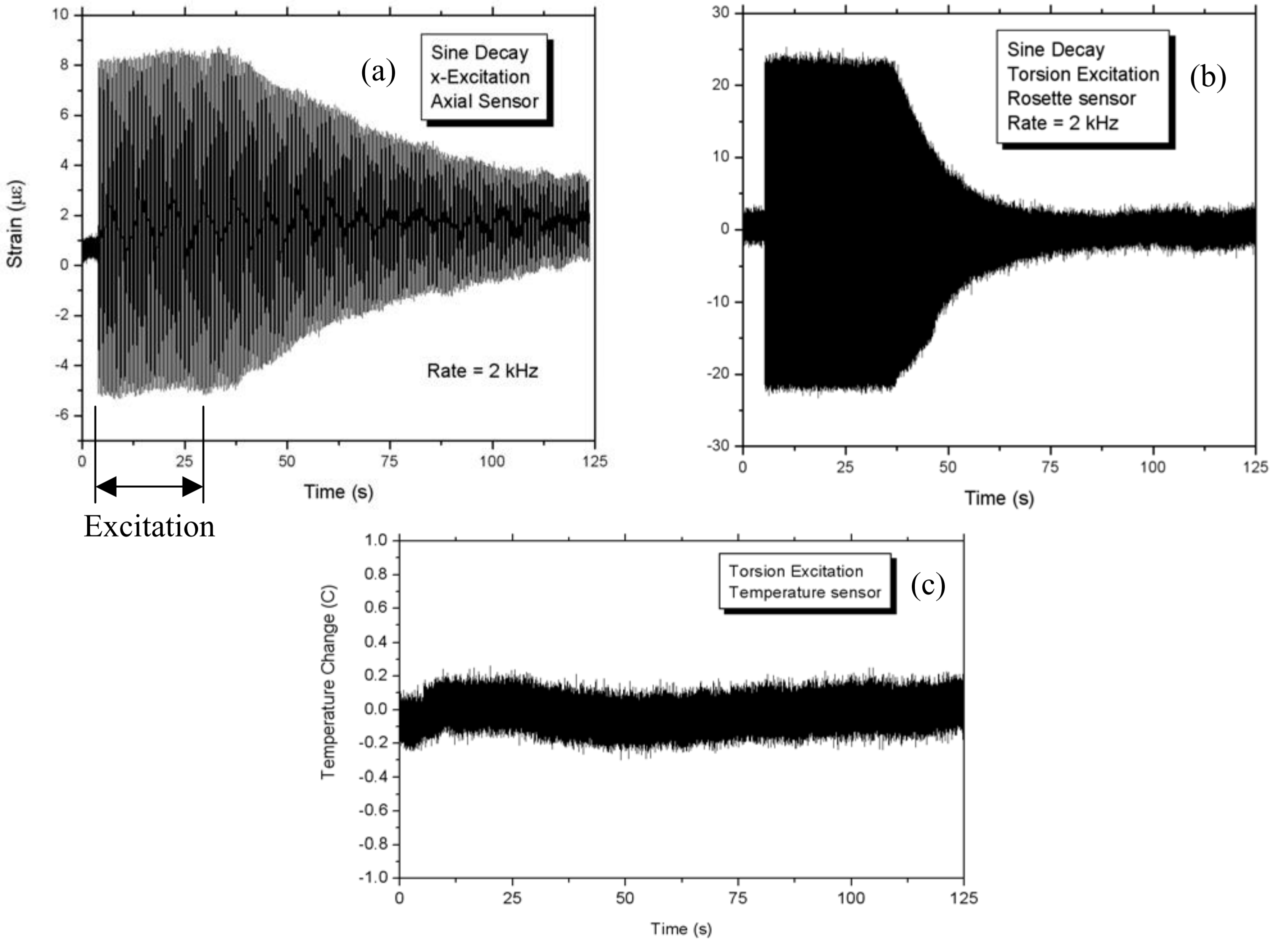

Figure 8. Strain (a,b) and temperature (c) data acquired during sine decay tests of the spacecraft latch.

The successful operation of the FBG distributed strain and temperature sensor system during its 5 months of data acquisition established the stiffness properties of the spacecraft latch under a wide range of loading conditions. The system demonstrated superior sensitivity and data quality and lower noise compared to electrical sensors, and the large amount of data was processed in a form that could be readily used for exhaustive mechanical analysis and modeling. Of particular note was the fact that the data were acquired at a high rate simultaneously from all sensors so that there was no time skew. The strain data measured by the FBG system were synched to the actuation and electrical sensor recordings such that precise comparisons of strain and acceleration could be made. The results of this test further confirm utility of FBG distributed strain sensors for spacecraft applications. Although this was a ground test, all components of the system either have been or could be space qualified for in-flight deployment.

3. INTERFEROMETRIC FIBER OPTIC GYROSCOPES

IFOGs are rotation sensors that can be used to measure spacecraft pointing and attitude; the performance of navigation-grade IFOGs in a benign environment is approaching the most stringent specifications for spacecraft. Figure 9 contains a simplified drawing of an IFOG. Based on a Sagnac interferometer, light of wavelength λ_o travels in opposite directions in a coil of optical fiber of length L and diameter D[8]. The Sagnac equation relates the optical phase shift ϕ_s of the two counter-propagating beams to the rotation rate Ω,

$$\phi_s = G\Omega = \frac{2\pi LD}{\lambda_o c_o}\Omega, \tag{1}$$

where c_o is the speed of light in vacuum. An IFOG achieves high rotation sensitivity by maximizing the LD product. Although the coil diameter is obviously limited by the available space for the IFOG, the length of fiber can be maximized; high performance gyros may have as much as 5-7 km of fiber in their sensor coil. To eliminate noise associated with polarization fading, these gyros use polarization-maintaining (PM) fiber. A number of performance issues, such as angle random walk (ARW), angle white noise (AWN), bias stability, and rate random walk (RRW), depend directly on the optical power on the detector, so it is advantageous to increase the light source power. However, the relative intensity noise (RIN) is inversely proportional to the bandwidth of the light. An elegant solution is to use an Er-doped fiber (EDF) light source[9], which can be configured as a two stage seed-amplifier to provide >100 mW output with an effective bandwidth in excess of 35 nm. In this case, λ_o in Eq. (1) is replaced by the interferometric or centroid wavelength λ_c.

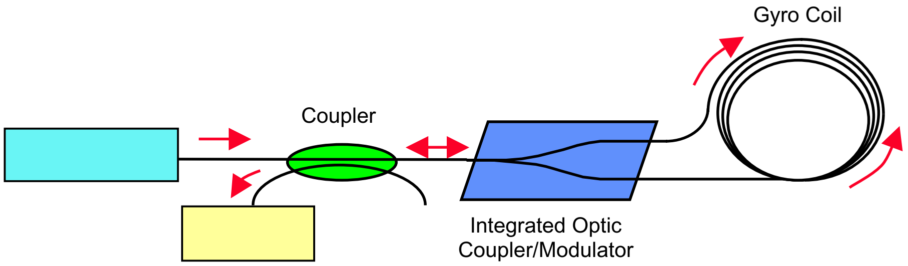

Figure 9. Simplified schematic drawing of an interferometric fiber optic gyroscope

Fiber optic data links have been shown to be extremely reliable in the space radiation environment, as described above, but IFOGs have radiation vulnerabilities that will have to be addressed before they can be used in low earth orbit (LEO) or mid earth orbit (MEO) where the flux of electrons and protons from the Van Allen belts is high. There are two principal effects of radiation on an IFOG[10]: 1) Radiation-induced absorption in the fiber components, which causes decreased optical power on the detector, resulting in decreased bias stability and increased ARW, AWN and RRW; and 2) Apparent shift in the wavelength of the broadband light, which causes a change in the scale factor relating optical phase shift to rotation rate. The former effect is exacerbated by the long length of fiber in the gyro coil and, to a lesser extent, the radiation sensitivity of the EDF in the fiber light source (FLS). The latter is due to radiation-induced changes in the FLS output spectrum and the filtering effect by the wavelength-dependent radiation-induced attenuation in the gyro coil.

3.1. Radiation induced loss in the PM gyro coil

Because of the long fiber length in the gyro coil, it is essential to minimize the radiation-induced attenuation to maintain gyro performance over the spacecraft lifetime. Conventional PM fibers, which have unacceptable radiation sensitivity as will be discussed below, consist of a Ge-doped silica core with a pure or doped silica optical cladding, similar to the structure of conventional telecom single mode fiber. However, PM fibers also have stress members in their structure, which induce birefringence in the core, breaking the degeneracy between the propagation constants for the two polarization states of light in the core. Thus, light launched into the fiber in one polarization state is inhibited from coupling into the other.

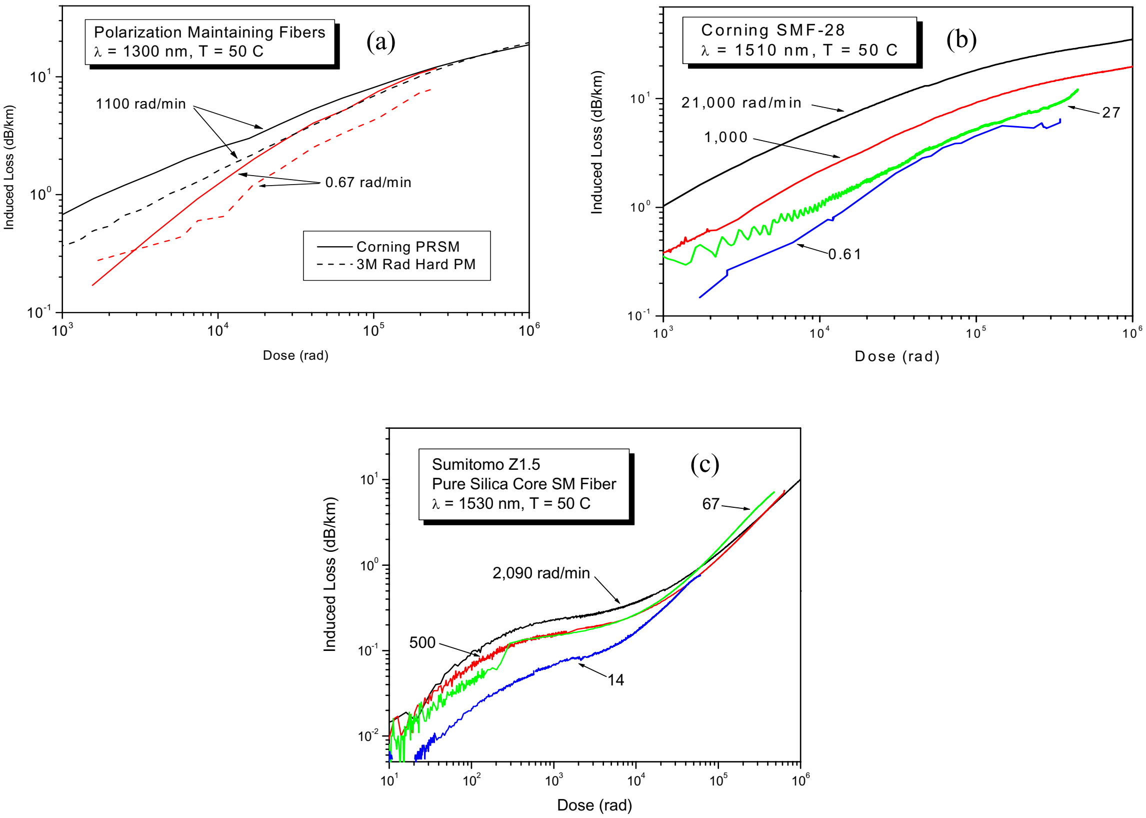

Figure 10. Growth of the radiation-induced attenuation during exposure to ^{60}Co γ-rays at various dose rates in (a) PM fibers at 1300 nm, (b) Corning SMF-28 Ge-doped silica core fiber at 1510 nm, and (c) Sumitomo Z1.5 pure silica core fiber measured in-situ at 50 C. The data in (a) and (b) were obtained using LED light sources; that in (c) was obtained with a broadband Er-doped FLS.

In general, the radiation sensitivity of Ge-doped silica core PM fibers is similar to that of single mode (SM) fibers[11] with the same core and cladding compositions. Figure 10 shows the growths of the radiation-induced losses in 3 Ge-doped silica core fibers: two PM fibers circa early 1990's and Corning SMF-28, which is a standard SM telecom fiber. Several observations can be made about these data: First, the induced loss is a very weak function of dose rate. A decrease in dose rate by a factor of ~2000 from 1,000 to ~0.6 rad/min results in only a factor of ~2 decrease in induced loss in the 3M and Corning SMF-28 fibers. An additional factor of ~10 decrease in dose rate in SMF-28 (data not shown) to ~0.05 rad/min results in only an additional 25% decrease in induced loss. (The dose rate dependence of fibers such as SMF-28 has been successfully modeled, allowing extrapolation to lower dose rates[12,13,14,15].) Second, the radiation-induced losses in these fibers are unacceptable for a lifetime, on-orbit dose of 10^5 rad. Using the 0.6 rad/min data as a worst case approximation of the 0.02 rad/min nominal on-orbit dose rate due to an exposure of 10^5 rad over 10 years, the incremental losses in the Corning PRSM, 3M PM, and SMF-28 fibers are 7.2, 4.3, and 4.5 dB/km, respectively. (Note that the PM fiber data were measured at 1300 nm vs. 1510 nm for SMF-28. The Er-doped FLS will spectrum spans a wavelength range of ~1520 – 1580 nm.) In a 5 km gyro coil, the worst-case end-of-life attenuation in the gyro coils would be ~20-35 dB, which would render the gyro inoperable. Clearly, the radiation response of these Ge-doped silica core fibers is unacceptable for this application. Third, processing and composition have a significant effect on the radiation damage. In Figure 10(a) the induced losses of the PRSM fiber at the two dose rates converge with increasing dose, but this effect is not evident in the other fibers.

It is well known that the radiation response of pure silica core fibers is significantly less than that in doped core fibers[16] and is sensitive to processing and impurities[17]. The relatively large concentration of core dopant provides a reservoir of traps for the radiolytic electrons and holes, whereas the traps in pure silica, which is intrinsically radiation hard, are largely due to vacancies and interstitials or impurities. Pure silica core fibers are used wherever possible in high radiation environments[18] such as nuclear reactors[19], or fusion reactors.[20] The Sumitomo Z fiber is probably the most radiation resistant pure silica core single mode fiber, and Figure 10(c) shows the growth of the radiation-induced losses in this fiber for several dose rates. The data are quite unusual—whereas there is a very slight dose rate dependence for doses $<10^5$ rad, the induced loss appears to be dose rate independent at higher doses. To the authors' knowledge, this behavior has not been previously reported, and current models of radiation damage cannot be used for prediction of induced loss at lower doses in this fiber. The implication of this dose rate independence, which needs to be verified at lower dose rates and with other radiation-hard pure silica core fibers, is that testing at laboratory dose rates is equivalent to on-orbit behavior and that the incremental loss will not be less at the lower dose rates.

The induced loss at 10^5 rad in the Sumitomo Z fiber is only ~1.3 dB/km, resulting in ~6-7 dB loss in a 5 km gyro coil, which could be compensated by increasing the light source fiber. The radiation response of the Sumitomo Z fiber is the Rosetta stone for other fibers' performance. Thus, the goal is to develop a pure silica core PM fiber possessing the good radiation hardness of the Z fiber together with intrinsic properties optimized for gyro coil. These include small fiber diameter to minimize the size of the gyro coil, low microbend loss to minimize the effect of fiber crossovers in the coil, and high birefringence to minimize polarization cross coupling. High birefringence implies close proximity of the stress members to the core, but they must be sufficiently distant to prevent interaction of the optical field with the highly radiation sensitive glass in the stress members. Further, the refractive index of the stress members must be less than that of the cladding to prevent secondary waveguiding. Low microbend loss dictates significant down doping of the cladding, in excess of that in the Z fiber, to more tightly confine the optical mode to the core ($\Delta n > 0.01$), but the achievable index difference is constrained by the limited concentration of fluorine that can be incorporated into silica. Obtaining these properties in an 80-μm fiber, which is beneficial for maintaining reasonable coil size, is a significant challenge for fiber design, and fabrication and will involve a number of trade-offs.

3.2. Radiation effects on the fiber light source

As described above, FLS optical power output of at least ~100 mW is necessary to minimize ARW, RRW and AWN and maximize bias stability. Additional requirements include broad bandwidth to minimize RIN and centroid wavelength stability to maintain a constant scale factor. A critical point is that these requirements must be met both at the beginning and end of the life of the spacecraft IFOG. It is also desirable to have an intrinsically polarized FLS output for efficient coupling to the integrated optic coupler/modulator (Figure 9), which inherently supports only one polarization. In terms of overall power consumption, which is critical on spacecraft, the best approach is to polarize the light after the oscillator stage in the FLS and then amplify the polarized light using PM EDF.

Figure 11 shows the degradation in optical power and the centroid wavelength shift for a FLS during irradiation. The induced loss is slightly dose rate dependent, which has been modeled by Williams et al.[21] using an exponential trap model. It should be noted that this source was pumped at 1488 nm; the induced loss would be significantly greater were it pumped at 980 nm due to the greater radiation-induced absorption in the EDF at the shorter pump wavelength. The power degradation follows a power law of dose, and even at this relatively high dose rate, there is only a 3 dB decrease after a dose of 150 krad. A more significant effect is seen in Figure 11(b), where a very large, unacceptable centroid shift is evident. This is due to change in the FLS spectrum, shown as the inset in Figure 11(b), which consists of at least 3 bands with differing radiation responses. The loss in optical power can be attributed primarily to color center absorption in the EDF due to radiation-sensitive dopants that are incorporated to optimize the intrinsic properties of the fiber for light source and amplifier applications[22], while the centroid wavelength shift is due to the differing radiation responses of the Er emission bands. It should be noted that HG-980, the fiber in this FLS, is a commercial product that is not optimized for radiation hardness.

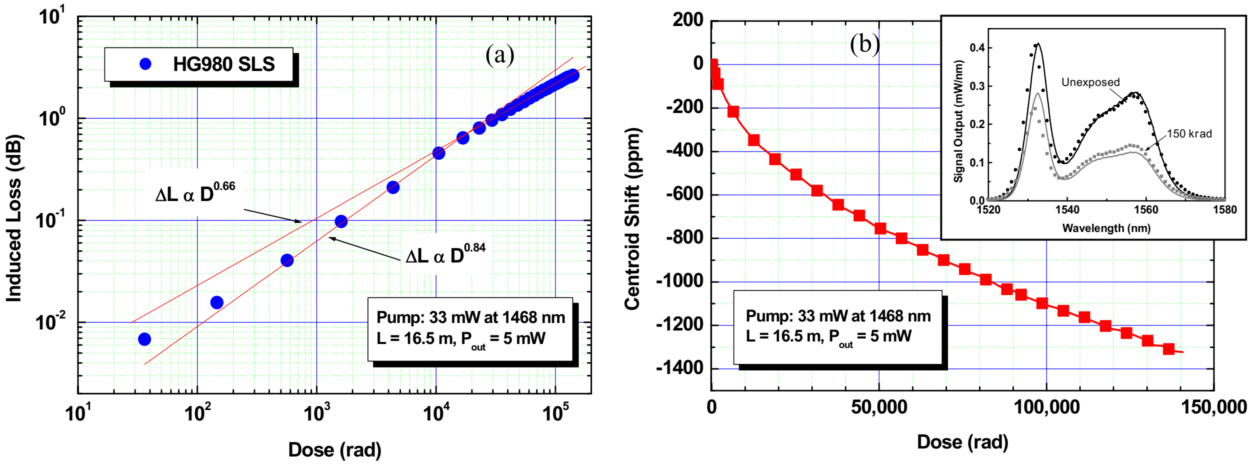

Figure 11. Radiation-induced power loss (a) and centroid wavelength shift (b) during a 35 rad/min ^{60}Co radiation exposure of a single stage superluminescent light source made with standard Lucent HG-980 erbium-doped fiber. The inset in (b) contains the measured (lines) and calculated (points) output spectra before and after radiation exposure.

4. CHALLENGES

There are several challenges that must be overcome before optical fiber sensors will find wide application onboard spacecraft. In the case of FBG strain sensing, the interrogation instrumentation must be made rugged, miniaturized, and space-qualified, and although there do not appear to be any show-stoppers, this will require a significant engineering effort. A more difficult task is for the spacecraft community to achieve sufficient experience and level of comfort with this technology to eliminate reluctance to deploy it. At the present time, the most significant driver for choosing fiber optic sensing is a critical measurement requirement that cannot be met by conventional, electrical strain gages, either because of technical or cost limitations. It is in these cases that fiber optic sensors have demonstrated their advantages.

In the case of the IFOG, the principal challenges are technical—both the sensor coil and EDF must be hardened against the space radiation environment. Two improvements are needed for the coil fiber: 1) Development of a pure silica core PM fiber with radiation hardness equivalent to that of the Sumitomo Z single mode fiber; and 2) Addressing the tradeoff between birefringence and mode confinement in an 80 μm fiber. The FLS presents the dual challenge of radiation hardening the EDF through composition and processing changes and developing schemes for compensating the output power loss and centroid wavelength shift over the on-orbit life of the spacecraft.

5. ACKNOWLEDGEMENTS

The authors thank Kenneth A. LaBel, NASA GSFC for helpful discussions, Sarah Glynn Arzt, formerly of NRL, for her technical assistance and Gary L. Young, Leonard Demchak, and Greg Lehr, Lockheed Martin, for their support and numerous contributions in testing the spacecraft latch.

6. REFERENCES

[1] E.W. Taylor, "Performance of the first operable fiber optic systems in prolonged space orbit," Small Satellite Technologies and Applications, SPIE Vol. 1691 (SPIE, Bellingham, WA, 1992), pp. 2-16.
[2] K.A. LaBel, P.W. Marshall, C.J. Marshall, J. Barth, H. Leidecker, R. Reed, and C.M. Seidleck, "Comparison of MIL-STD-1773 fiber optic data bus terminals: Single event proton irradiation, in-flight space performance, and prediction techniques, IEEE Trans. Nucl. Sci. 45 (1998) 1633-1639 and references therein.

[3] A.D. Kersey, M.A. Davis, H.J. Patrick, M. LeBlanc, K.P. Koo, C.G. Askins, M.A. Putnam and E.J. Friebele, "An overview of fiber grating sensors," J. Lightwave Tech. 15 (1997) 1442-1463.

[4] E.J. Friebele, C.G. Askins, A.B. Bosse, A.D. Kersey, H.J. Patrick, W.R. Pogue, M.A. Putnam, W.R. Simon, F.A. Tasker, W.S. Vincent and S.T. Vohra, "Optical fiber sensors for spacecraft applications," Smart Materials and Structures 8 (1999) 1-26.

[5] C.G. Askins, M.A. Putnam, G.M. Williams and E. J. Friebele, "Stepped-wavelength optical-fiber Bragg grating arrays fabricated in line on a draw tower" Optics Lett. 19 (1994) 147-149.

[6] C.G. Askins, M. A. Putnam and E.J. Friebele, "Instrumentation for interrogating many-element fiber Bragg grating arrays", Smart Sensing, Processing and Instrumentation, SPIE Vol. 2444, W.B. Spillman, Jr., Ed. (SPIE, Bellingham, WA, 1995), pp. 257-266.

[7] US Pat. # 6233373, "Optical spectrometer with improved geometry and data processing for monitoring fiber Bragg gratings"

[8] H. Lefevre, "The Fiber-Optic Gyroscope," Artech House (Boston, 1993).

[9] D.C. Hall, W.K. Burns, and R.P. Moeller, "High-stability Er^{3+}-doped superfluorescent fiber sources," J. Lightwave Tech. 13 (1995) 1452-1460.

[10] G.M. Williams and E.J. Friebele, "Space radiation effects on erbium-doped fiber devices: sources, amplifiers and passive measurements," IEEE Trans. Nucl. Sci. 45 (1998) 1531-1536.

[11] E.J. Friebele, L.A. Brambani, M.E. Gingerich, S.J. Hickey and J.R. Onstott, "Radiation-induced attenuation in polarization-maintaining fibers: Low dose rate response, stress and materials effects," Appl. Opt. 28 (1989) 5138-5143.

[12] E.J. Friebele, M.E. Gingerich and D.L. Griscom, "Survivability of optical fibers in space," Optical Materials Reliability and Testing (SPIE Vol. 1791), R.A. Greenwell, Ed. (SPIE, Bellingham, WA, 1992) pp. 177-188.

[13] D.L. Griscom, M.E. Gingerich and E.J. Friebele, "Radiation-induced defects in glasses: Origin of power-law dependence of concentration on dose," Phys. Rev. Lett. 71 (1993) 1019-1022.

[14] D.L. Griscom, M.E. Gingerich and E.J. Friebele, "Model for the dose, dose-rate and temperature dependence of radiation-induced loss in optical fibers," IEEE Trans. Nucl. Sci. 41 (1994) 523-527.

[15] D.L. Griscom, "Fractal kinetics of radiation-induced point-defect formation and decay in amorphous insulators: Application to color centers in silica-based optical fibers," Phys. Rev. B 64 (2001) 174201-1-14.

[16] E.J. Friebele, C.G. Askins, M.E. Gingerich, and K.J. Long, "Optical fiber waveguides in radiation environments, II," Nucl. Inst. Meth. in Phys. Res. B1 (1984) 355-369.

[17] E.J. Friebele, M.E. Gingerich, K.J. Long, P.S. Levin, and D.A. Pinnow, "Radiation-resistant low OH content silica core fibers," IEEE J. Lightwave Tech. LT-1 (1983) 462-465.

[18] H. Henschel, O. Kohn, and U. Weinand, "A new radiation hard optical fiber for high-dose values," IEEE Trans. Nucl. Sci. 49 (2002) 1432-1438.

[19] D.W. Miller, D.E. Holcomb, H. Shao, J.W. Talnagi, and J.M. Hatch, "Optical Fibers in Radiation Environments," Electric Power Research Institute Report TR-100367, Palo Alto, CA, 1992.

[20] D.L. Griscom, "γ and fission-reactor radiation effects on the visible-range transparency of aluminum-jacketed, all-silica optical fibers," J. Appl. Phys. 80 (1996) 1-14.

[21] G.M. Williams, B.M. Wright and E.J. Friebele, "Effect of space environment radiation exposure of erbium-doped fiber amplifiers and superluminescent sources," Optical Fiber Reliability and Testing, SPIE Vol. 3848, M.J. Matthewson, Ed. (SPIE, Bellingham, WA, 1999), pp. 271-280.

[22] G.M. Williams, M.A. Putnam, C.G. Askins, M.E. Gingerich and E.J. Friebele, "Radiation effects in erbium-doped optical fibres," Elect. Lett. 28 (1992) 1816-1818.

*friebele@nrl.navy.mil; phone 1 202 767 2270; fax 1 202 767 5792; nrl.navy.mil